Available online at www.sciencedirect.com
ScienceDirect
Journal of Sound and Vibration 299 (2007) 298–313
JOURNAL OF SOUND AND VIBRATION
www.elsevier.com/locate/jsvi

In-plane vibration of thin elliptic plates submitted to uniform pulsed microwave irradiations

A.R. Hadj Henni*, C. Bacon

Laboratoire de Mécanique Physique, Bordeaux 1 University, UMR C.N.R.S. 5469, 351 cours de la Libération, 33405 Talence Cedex, France

Received 22 March 2006; received in revised form 24 July 2006; accepted 8 August 2006
Available online 25 September 2006

Abstract

The technique of acoustic generation by microwave excitation in structures is applied here to study the in-plane vibration of full or hollowed elliptic plates. The absorption of pulsed microwave irradiations by a material causes a sudden rise of its temperature and the generation of an acoustic wave by thermoelastic effect. A semi-analytic theoretical model is developed to predict the in-plane displacement fields in elliptic thin plates submitted to a uniform temperature rise. It is assumed that the isotropic and viscoelastic plate constitutive material is submitted to a thermoelastic excitation under a plane stress state. The wave equations that govern the Helmholtz displacement potentials are resolved in an elliptic cylindrical system of coordinates by means of infinite angular and radial Mathieu functions series. The displacement field is finally obtained by taking into account the zero stress conditions on the boundaries of the plates. The comparison between the theoretical and the experimental responses of full and hollowed elliptic plates shows a good agreement that permits the validation of the developed model.

1. Introduction

Many authors have studied the vibration and acoustic propagation problems in elliptic structures since the pioneering works of Mathieu [1] on the vibration of elliptic membranes in the nineteenth century. Indeed, various problems involving scalar fields governed by the wave differential equation in an elliptic geometry have been treated in the literature [2,3]. By assuming different boundary conditions, the vibration of elliptic plates has been studied in the case of out-of-plane flexural vibration by analytically solving the Mathieu equations [4–6] or by using the Rayleigh–Ritz method [7]. Furthermore, the propagation of elastic waves in infinite elliptic cylinders and diffraction problems has been treated since the works of Barakat [8] and Wong et al. [9]. In the opposite, no studies about the in-plane vibration of elliptic plates have been found in the literature.

The aim of the present work is to study theoretically and experimentally the in-plane vibration of full and hollowed thin elliptic plates excited by uniform pulsed microwaves. Indeed, this recent technique [10] permits to generate elastic waves in the plane of an irradiated plate. Physically, the absorption of electromagnetic

*Corresponding author. Tel.: +33 540 008 930; fax: +33 540 006 964.
E-mail address: ar.hadjhenni@lmp.u-bordeaux1.fr (A.R. Hadj Henni).

0022-460X/$ - see front matter © 2006 Elsevier Ltd. All rights reserved.
doi:10.1016/j.jsv.2006.08.004

irradiations by a material, that must be sufficiently non-conductive, causes an agitation of its molecular structure, which induces an increase of temperature. By a thermal expansion, this latter produces elastic waves which induces the in-plane vibration of the irradiated plate. The acoustic generation by pulsed microwaves has been successfully applied to study the vibration of one-dimensional structures [11–13] and to evaluate mechanical and electromagnetic properties of different elastic and dielectric materials [14–19]. The main advantage of the microwave generation technique is that this kind of volumic generation allows producing quasi-perfect in-plane vibrations. Indeed, the plates used here are quite thin and, since the microwave absorption is very low for the materials used in this work, the temperature rise is almost uniform in the plate thickness.

A theoretical model will be developed to predict the vibration of full or hollowed elliptic plates under the action of a uniform microwave excitation. Considering the elliptic geometry of the studied thin plates, an elliptic cylindrical system of coordinates [20,21] will be adopted to formulate and to solve the problem. Assuming a plane stress state and considering the material as viscoelastic and isotropic, the adapted Navier displacement equation [21,22] will be solved by applying a Helmholtz decomposition into potentials to the displacement field. In the elliptic cylindrical system of coordinates, the solutions of the obtained wave equations will be expressed as infinite series of angular and radial Mathieu functions products [23,24]. These latter will be briefly presented since their use is not very widespread. By taking into account the zero stress boundary conditions and by applying an angular discretization to the plate boundaries, the problem will be reduced to the resolution of a linear system of equations.

Finally, the comparison between the experimental and the theoretical displacement fields in full and hollowed elliptic plates will permit to validate the model. The extension of the model developed here to the case of infinite elliptic cylinders will also be explained.

2. Theory

2.1. Problem formulation and wave equations

The in-plane vibration of full and hollowed thin elliptic plates is studied by calculating the displacement fields. The constitutive material of the plates is assumed to be linearly viscoelastic. The behavior law expression of such material in the time domain uses convolution products that are transformed to classical products in the frequency domain. Consequently, in the following developments, one can choose to express all the quantities in the frequency domain by applying a Fourier transform to the variables expressed in the time domain. The angular pulsation ω will not appear in the developments; nevertheless any exception will be mentioned. In addition, since the material is supposed to be viscoelastic, its mechanical characteristics are represented by complex coefficients in order to take into account the viscosity attenuation.

Considering the geometry and the symmetry of the studied structures, one can use the elliptic cylindrical system of coordinates, represented in Fig. 1, to formulate the problem. In the orthogonal coordinate system $(O, \mathbf{e}_\xi, \mathbf{e}_\eta, \mathbf{e}_z)$, any point is defined by the intersection of an ellipse ξ, of a hyperbole η and of a z-axis. The elliptic coordinates are related to the Cartesian ones by the following relations [20]:

$$x = f\ \cosh\ \xi\ \cos\ \eta, \quad y = f\ \sinh\ \xi\ \sin\ \eta \quad \text{and} \quad z = z. \tag{1}$$

By calling a and b the lengths of the major and the minor semi-axes of an ellipse, respectively, the semi-interfocal distance $f = \sqrt{a^2 - b^2}$ is identical for all ellipses and hyperbola defined in a same elliptic system of coordinates. Finally, the scale factors h_i of a such coordinate system is given by [20]

$$h_1^2 = h_2^2 = h^2 = f^2\left(\sinh^2 \xi + \sin^2 \eta\right) \quad \text{and} \quad h_3^2 = 1. \tag{2}$$

We consider a two-dimensional problem of a thin plate submitted to in-plane stresses. If the thickness of a plate is small compared to the wavelengths involved (low frequency range), then a plane stress state can be considered. Here, the plane stress assumption to model the vibration of thin elliptic plates is justified by the small thickness of the experimentally tested plates (see Section 4) and the considered frequency range.

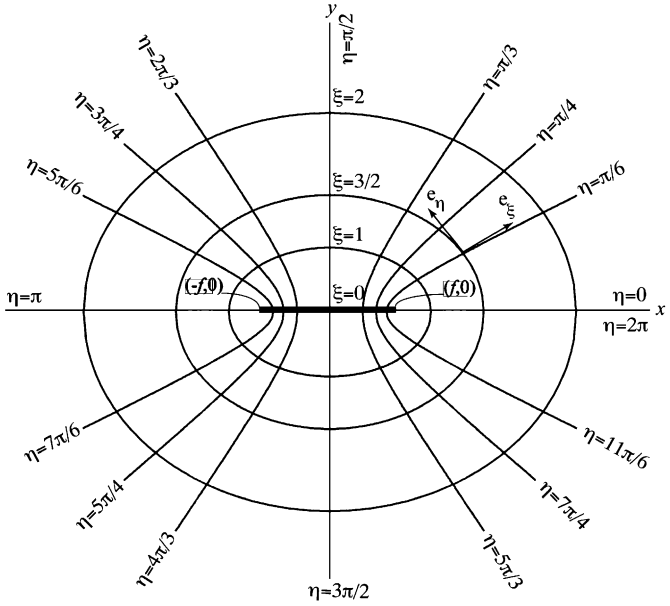

Fig. 1. Elliptic cylindrical system of coordinates.

The aim of the modeling is to calculate both components of the displacement field in the plane of the plates $(\mathbf{e}_\xi, \mathbf{e}_\eta)$. Consequently, one can choose for the displacement in this plane the following:

$$\mathbf{U} = \begin{pmatrix} U_\xi(\xi,\eta) & U_\eta(\xi,\eta) \end{pmatrix}^{\mathrm{T}}. \tag{3}$$

It can be noticed that this displacement field corresponds only to the in-plane part of the total displacement, even if a transverse displacement U_z exists. This transverse displacement is due to the Poisson effect and to the thermal expansion. The component U_z does not appear in the following equations but it is taken into account in the calculation of the material coefficients used in Eq. (4).

As it will be carried out in the experimental setup (Section 4), the plate is submitted to a sudden rise of temperature $\Delta T(\xi,\eta)$ that is assumed to be symmetric with respect to the axis $\eta = 0$ of the plate plane. Under the hypothesis of a plane stress state, the components of the stress tensor $(\boldsymbol{\sigma})$ in the plane $(\mathbf{e}_\xi, \mathbf{e}_\eta)$ are given by

$$\begin{aligned} \sigma_{\xi\xi} &= Q_{11}\varepsilon_{\xi\xi} + Q_{12}\varepsilon_{\eta\eta} - B_1\Delta T(\xi,\eta), \\ \sigma_{\eta\eta} &= Q_{12}\varepsilon_{\xi\xi} + Q_{22}\varepsilon_{\eta\eta} - B_2\Delta T(\xi,\eta), \\ \sigma_{\xi\eta} &= 2Q_{66}\varepsilon_{\xi\eta}, \end{aligned} \tag{4}$$

where ε_{ij} are the in-plane components of the strain tensor $\boldsymbol{\varepsilon}$ defined by the following kinematic expression:

$$2\boldsymbol{\varepsilon} = \nabla\mathbf{U} + (\nabla\mathbf{U})^{\mathrm{T}}. \tag{5}$$

The coefficients Q_{ij} (components of the reduced rigidity matrix) and B_i are defined by considering the plane stress state, i.e. the σ_{zz} stress component is zero.

In addition, if the material is supposed to be isotropic and designating by E, v and α, respectively, the complex Young's modulus, the Poisson's ratio and the coefficient of thermal dilatation, then the coefficients Q_{ij} and B_i are defined by

$$Q_{11} = Q_{22} = \frac{E}{1-v^2}, \quad Q_{12} = Q_{21} = \frac{Ev}{1-v^2}, \quad Q_{66} = \frac{E}{2(1+v)} \quad \text{and} \quad B_1 = B_2 = \frac{E}{1-v}\alpha. \tag{6}$$

It is possible to rewrite Eq. (4) in a contracted way as follows:

$$\boldsymbol{\sigma} = Q_{12}(\nabla\cdot\mathbf{U})\mathbf{I} + \big(Q_{11} - Q_{12}\big)\boldsymbol{\varepsilon} - \mathbf{B}_1\Delta T(\xi,\eta)\mathbf{I}, \tag{7}$$

where $\mathbf{I}$ is the identity tensor.

The field function $\Delta T(\xi,\eta)$ is the Fourier transform of the temperature rise in the material due to the absorption of microwave irradiations. If the temperature rise is assumed to be sudden in comparison with the duration of the mechanical response and occurs without conduction and dissipation, then the temporal form of $\Delta T(\xi,\eta)$ can be expressed by

$$\Delta T(t,\xi,\eta) = \Delta T(\xi,\eta) f(t), \tag{8}$$

where $\Delta T(\xi,\eta)$ represents the space distribution of the temperature rise and $f(t)$ the temporal evolution that can be modeled by a step function if the duration of the microwave heating is very small compared to the test duration.

In the case of an infinite elliptic cylinder, one can note that the hypothesis of a plane stress state is replaced by the hypothesis of a plane strain state [21,22]. Eq. (4) will keep the same form if the coefficients Q_{ij}, given in Eq. (6), are replaced by the coefficients C_{ij} of the material complex stiffness matrix $\mathbf{C}$. If the excitation source is adapted to excite cylinders uniformly along their axes in order to verify the plane strain hypothesis, then the method presented in what follows for thin elliptic plates can be used in the same way for studying the vibration of infinite elliptic cylinders and pipes.

The combination of the behavior law in Eq. (7), the kinematic relation in Eq. (5) and the local equilibrium equation

$$\nabla \cdot \boldsymbol{\sigma} = -\rho\omega^2 \mathbf{U}, \tag{9}$$

permits to obtain the Navier displacement differential equation corresponding to a plane stress state

$$Q_{11}\nabla(\nabla \cdot \mathbf{U}) - \frac{Q_{11}-Q_{12}}{2}\nabla \times (\nabla \times \mathbf{U}) + \rho\omega^2 \mathbf{U} = B_1 \nabla(\Delta T(\xi,\eta)). \tag{10}$$

The resolution of this differential equation depends on the space distribution of the temperature rise, which is itself related to the microwave excitation field. The knowledge of the excitation field is necessary to formulate the researched solution as the sum of a homogeneous solution and a particular one. Considering the difficulty to predict the temperature spatial distribution, the displacement field will be determined only for a uniform temperature rise ΔT. In this case, the temperature rise gradient is null and Eq. (10) becomes homogenous and analytically solvable:

$$Q_{11}\nabla(\nabla \cdot \mathbf{U}) - \frac{Q_{11}-Q_{12}}{2}\nabla \times (\nabla \times \mathbf{U}) + \rho\omega^2 \mathbf{U} = 0. \tag{11}$$

A Helmholtz decomposition into potentials [21,22] can be applied to the displacement field of Eq. (11),

$$\mathbf{U} = \nabla\varphi + \nabla \times \boldsymbol{\psi}, \tag{12}$$

where φ and $\boldsymbol{\psi}$ are the scalar and the vectorial potentials of the displacement, respectively. Since the displacement field $\mathbf{U}$ does not depend on the z coordinate, the vector $\boldsymbol{\psi}$ has the following form:

$$\boldsymbol{\psi} = \begin{pmatrix} 0 & 0 & \psi(\xi,\eta) \end{pmatrix}^{\mathrm{T}}. \tag{13}$$

Both Helmholtz potentials have to verify the following wave equations:

$$\begin{aligned} \nabla^2\varphi + k_L^2\varphi &= 0, \\ \nabla^2\boldsymbol{\psi} + k_T^2\boldsymbol{\psi} &= 0, \end{aligned} \tag{14}$$

where $k_L = \omega/c_L$, $k_L = \omega/c_T$, and $c_L^2 = Q_{11}/\rho$, $c_T^2 = Q_{66}/\rho$ are the longitudinal and transverse wavenumbers, and the longitudinal and transverse wave velocities in the material, respectively.

The development of Eq. (12) in the elliptic cylindrical system of coordinates gives the following displacement field components:

$$\begin{aligned} U_\xi(\xi,\eta) &= \frac{1}{h}\left(\frac{\partial\varphi}{\partial\xi} + \frac{\partial\psi}{\partial\eta}\right), \\ U_\eta(\xi,\eta) &= \frac{1}{h}\left(\frac{\partial\varphi}{\partial\eta} - \frac{\partial\psi}{\partial\xi}\right). \end{aligned} \tag{15}$$

The differential equations in Eq. (14) are Helmholtz equations, solvable in the elliptic system of coordinates by the technique of separation of variables [21,22].

2.2. Resolution of the Helmholtz equations in an elliptical system of coordinates

The development of the Laplace operator in an elliptic coordinate system allows rewriting the Helmholtz Eqs. (14) as follows:

$$\frac{1}{f^2(\sinh^2\xi+\sin^2\eta)}\left(\frac{\partial^2\varphi}{\partial\xi^2}+\frac{\partial^2\varphi}{\partial\eta^2}\right)+k_L^2\varphi=0,$$
$$\frac{1}{f^2(\sinh^2\xi+\sin^2\eta)}\left(\frac{\partial^2\psi}{\partial\xi^2}+\frac{\partial^2\psi}{\partial\eta^2}\right)+k_T^2\psi=0. \tag{16}$$

Since the Helmholtz equation is separable in the elliptic system of coordinates [21–24], one can apply the technique of separation of variables to the functions φ and ψ. By calling $\varphi_\xi(\xi)$, $\psi_\xi(\xi)$, $\varphi_\eta(\eta)$ and $\psi_\eta(\eta)$ the radial and the angular parts of the potentials φ and ψ, respectively, such as $\varphi(\xi,\eta)=\varphi_\xi(\xi)\varphi_\eta(\eta)$ and $\psi(\xi,\eta)=\psi_\xi(\xi)\psi_\eta(\eta)$, the following differential equations are found to be verified by each of the above functions:

$$\frac{\partial^2\varphi_\xi}{\partial\xi^2}-\left((c_\varphi+\frac{1}{2}f^2k_L^2)-\frac{1}{2}f^2k_L^2\cosh(2\xi)\right)\varphi_\xi=0,$$
$$\frac{\partial^2\varphi_\eta}{\partial\eta^2}+\left((c_\varphi+\frac{1}{2}f^2k_L^2)-\frac{1}{2}f^2k_L^2\cos(2\eta)\right)\varphi_\eta=0, \tag{17}$$

$$\frac{\partial^2\psi_\xi}{\partial\xi^2}-\left((c_\psi+\frac{1}{2}f^2k_T^2)-\frac{1}{2}f^2k_T^2\cosh(2\xi)\right)\psi_\xi=0,$$
$$\frac{\partial^2\psi_\eta}{\partial\eta^2}+\left((c_\psi+\frac{1}{2}f^2k_T^2)-\frac{1}{2}f^2k_T^2\cos(2\eta)\right)\psi_\eta=0, \tag{18}$$

where c_φ and c_ψ are separation constants. By defining the following parameters:

$$\alpha_L=c_\varphi+\frac{1}{2}f^2k_L^2,\quad \alpha_T=c_\psi+\frac{1}{2}f^2k_T^2,\quad q_L=\frac{1}{4}f^2k_L^2\quad\text{and}\quad q_T=\frac{1}{4}f^2k_T^2, \tag{19}$$

Eqs. (17,18) become

$$\frac{d^2\varphi_\eta}{d\eta^2}+[\alpha_L-2q_L\cos(2\eta)]\varphi_\eta=0,$$
$$\frac{d^2\varphi_\xi}{d\xi^2}-[\alpha_L-2q_L\cosh(2\xi)]\varphi_\xi=0, \tag{20}$$

$$\frac{d^2\psi_\eta}{d\eta^2}+[\alpha_T-2q_T\cos(2\eta)]\psi_\eta=0,$$
$$\frac{d^2\psi_\xi}{d\xi^2}-[\alpha_T-2q_T\cosh(2\xi)]\psi_\xi=0. \tag{21}$$

The differential equations that depend on η are angular (or ordinary) Mathieu equations, while those depending on the variable ξ are radial (or modified) Mathieu equations [23,24]. The solutions of these equations are, respectively, the angular and the radial Mathieu functions.

It is clear that the displacement field is a periodic function of η. The values of the parameters α_L and α_T that satisfy this condition are called the *characteristic values* [23,24] of the Mathieu functions and constitute infinite

sets ordered as follows:

$$\alpha_{L_0} < \alpha_{L_1} < \alpha_{L_2} < \cdots \quad \text{and} \quad \alpha_{T_0} < \alpha_{T_1} < \alpha_{T_2} < \cdots. \tag{22}$$

The characteristic values depend on the symmetry of Mathieu functions and, consequently, on the mechanical behavior of the studied plates. In the next, if the angular Mathieu functions are symmetric with respect to the axis $\eta = 0$ (even functions), then the n-order characteristic value will be designated by α_{L_n} or α_{T_n} ($n = 0, 1, 2, \ldots$). In the opposite, if the angular Mathieu functions are antisymmetric (odd functions), then the characteristic values become β_{L_n} or β_{T_n} ($n = 1, 2, 3, \ldots$). One can note that Mathieu functions of zero order are only even and symmetric with respect to the axis $\eta = 0$.

In the present work, the angular Mathieu functions will be designated in accordance with the notation used by Stratton [24] and Morse and Feshbach [21]. As for the radial Mathieu functions, their notations will be those used by Stratton [24]. One can note that the Mathieu functions depend on a geometrical variable (ξ or η) as well as on a parameter q (q_L or q_T) given in Eqs (19). Finally, the Mathieu functions will be calculated using a code based on the algorithms of Zhang and Jin [25].

2.3. Resolution of the differential equations for a hollowed elliptic plate

2.3.1. Potentials forms

In the elliptic system of coordinates $(O, \mathbf{e}_\xi, \mathbf{e}_\eta)$, the external boundary of the elliptic plate is ξ_2. This plate is hollowed by a confocal ellipse of coordinate ξ_1. The in-plane vibration of the plate is governed by the potential wave Eqs. (20) and (21). In what follows, only the research of the scalar potential $\varphi(\xi, \eta)$ will be detailed since the procedure remains the same for the vectorial potential $\boldsymbol{\psi}(\xi, \eta)$.

The solution function $\varphi_\eta(\eta)$ is a linear combination of angular Mathieu functions of first and second kinds. In the same way, the solution function $\varphi_\xi(\xi)$ is a linear combination of radial Mathieu functions of the two kinds. Considering the parity of the Mathieu functions and remembering that the potential is the product of its radial and angular parts, the n-order scalar function $\varphi_n(\xi, \eta)$ has the following form:

$$\begin{aligned}
\varphi_n(\xi,\eta) &= \left[A_n^J Je_n(q_L,\xi) + A_n^N Ne_n(q_L,\xi)\right]\left[A_n^S Se_n(q_L,\eta) + A_n^F Fe_n(q_L,\eta)\right], \quad n = 0, 1, 2 \ldots, \\
\varphi_n(\xi,\eta) &= \left[B_n^J Jo_n(q_L,\xi) + B_n^N No_n(q_L,\xi)\right]\left[B_n^S So_n(q_L,\eta) + B_n^F Fo_n(q_L,\eta)\right], \quad n = 1, 2, 3 \ldots.
\end{aligned} \tag{23}$$

It is possible to simplify the expressions in Eq. (23) by taking into account the physical conditions related to the vibration of an elliptic plate. Indeed, the displacement field and the potentials have to be periodic with respect to η (of period π or 2π depending on the parity of the order n). Since the second order angular Mathieu functions $Fe_n(q, \eta)$ and $Fo_n(q, \eta)$ are not periodic, they do not enter in the formulation of the potentials. In addition, the use of second kind radial Mathieu functions is justified by the presence of a material discontinuity in the hollowed plate [21].

In order to formulate the general solutions of Eqs. (14), the solutions of different orders and parities will be linearly composed. Finally, by renaming the non-zero coefficients, the potentials are expressed as infinite series of even and odd Mathieu functions:

$$\begin{aligned}
\varphi(\xi,\eta) = &\sum_{n=0}^{\infty}\left(A_n^\varphi Je_n(q_L,\xi) + B_n^\varphi Ne_n(q_L,\xi)\right)Se_n(q_L,\eta) \\
&+ \sum_{n=1}^{\infty}\left(C_n^\varphi Jo_n(q_L,\xi) + D_n^\varphi No_n(q_L,\xi)\right)So_n(q_L,\eta), \\
\psi(\xi,\eta) = &\sum_{n=0}^{\infty}\left(A_n^\psi Je_n(q_T,\xi) + B_n^\psi Ne_n(q_T,\xi)\right)Se_n(q_T,\eta) \\
&+ \sum_{n=1}^{\infty}\left(C_n^\psi Jo_n(q_T,\xi) + D_n^\psi No_n(q_T,\xi)\right)So_n(q_T,\eta),
\end{aligned} \tag{24}$$

where the coefficients A_n^φ, B_n^φ, C_n^φ, D_n^φ, A_n^ψ, B_n^ψ, C_n^ψ and D_n^ψ in the potentials of Eq. (24) depend on the boundary conditions of the problem.

Considering the spatial symmetry of the excitation assumed in the formulation of the problem, it appears that the following relations are verified in all angular and radial positions:

$$\begin{aligned} &U_\xi(\xi,\eta) = U_\xi(\xi,-\eta) \\ &U_\eta(\xi,\eta) = -U_\eta(\xi,-\eta) \end{aligned} \qquad \forall(\xi,\eta) \in [\xi_1,\xi_2]\times[0,2\pi]\ . \tag{25}$$

By taking into account Eq. (25) and after calculation, it appears that for any integer n,

$$A_n^\psi = B_n^\psi = C_n^\varphi = D_n^\varphi = 0. \tag{26}$$

By renaming the coefficients a last time, the potentials become:

$$\begin{aligned} \varphi(\xi,\eta) &= \sum_{n=0}^{\infty}\big(A_n Je_n(q_L,\xi) + B_n Ne_n(q_L,\xi)\big)Se_n(q_L,\eta), \\ \psi(\xi,\eta) &= \sum_{n=1}^{\infty}\big(C_n Jo_n(q_T,\xi) + D_n No_n(q_T,\xi)\big)So_n(q_T,\eta). \end{aligned} \tag{27}$$

In other words, the scalar and the vectorial potentials, $\varphi(\xi,\eta)$ and $\boldsymbol{\psi}(\xi,\eta)$, are even and odd functions of the angular variable η, respectively. Finally, the displacement field, given by Eq. (15), has the following form:

$$\begin{aligned} U_\xi(\xi,\eta) &= \frac{1}{h}\sum_{n=0}^{\infty}\big(A_n Je_n'(q_L,\xi) + B_n Ne_n'(q_L,\xi)\big)Se_n(q_L,\eta) \\ &\quad + \frac{1}{h}\sum_{n=1}^{\infty}\big(C_n Jo_n(q_T,\xi) + D_n No_n(q_T,\xi)\big)So_n'(q_T,\eta), \\ U_\eta(\xi,\eta) &= \frac{1}{h}\sum_{n=0}^{\infty}\big(A_n Je_n(q_L,\xi) + B_n Ne_n(q_L,\xi)\big)Se_n'(q_L,\eta) \\ &\quad - \frac{1}{h}\sum_{n=1}^{\infty}\big(C_n Jo_n'(q_T,\xi) + D_n No_n'(q_T,\xi)\big)So_n(q_T,\eta). \end{aligned} \tag{28}$$

The unknown coefficients A_n, B_n, C_n and D_n in Eq. (28) are determined by taking into account the zero stress boundary conditions at the boundaries of the structure.

2.3.2. Boundary conditions

Since the elliptic plate is free on its boundaries, the boundary conditions are given by the following:

$$\boldsymbol{\sigma}\cdot\mathbf{n}_i = \mathbf{0} \quad \text{at} \quad \xi = \xi_i \quad (i = 1,2), \tag{29}$$

where $\mathbf{n}_i$ is the outward unit vector normal to the boundary i.

The stress tensor components are related to the strains by Eq. (4). After calculation, the boundary conditions are expressed in terms of strains as follows:

$$\begin{aligned} &\varepsilon_{\xi\xi} + v\varepsilon_{\eta\eta} = (1+v)\alpha\Delta T \\ &\varepsilon_{\xi\eta} = 0 \end{aligned} \qquad \text{at} \quad \xi = \xi_i \quad (i = 1,2). \tag{30}$$

In other respects, the development of Eq. (5) gives the strain expressions in term of displacements,

$$\varepsilon_{\xi\xi} = \frac{1}{h}\left(\frac{\partial U_\xi}{\partial\xi} + \frac{1}{h}\frac{\partial h}{\partial\eta}U_\eta\right), \quad \varepsilon_{\eta\eta} = \frac{1}{h}\left(\frac{\partial U_\eta}{\partial\eta} + \frac{1}{h}\frac{\partial h}{\partial\xi}U_\xi\right)$$

and

$$\varepsilon_{\xi\eta} = \frac{1}{h}\left(\frac{\partial U_\xi}{\partial\eta} - \frac{1}{h}\frac{\partial h}{\partial\xi}U_\eta + \frac{\partial U_\eta}{\partial\xi} - \frac{1}{h}\frac{\partial h}{\partial\eta}U_\xi\right). \tag{31}$$

Consequently, the system of Eq. (30) becomes at $\xi = \xi_i$ $(i = 1, 2)$:

$$\sum_{n=0}^{\infty} f_n^J(q_L,\xi_i,\eta)A_n + \sum_{n=0}^{\infty} f_n^N(q_L,\xi_i,\eta)B_n + \sum_{n=1}^{\infty} g_n^J(q_T,\xi_i,\eta)C_n + \sum_{n=1}^{\infty} g_n^N(q_T,\xi_i,\eta)D_n = (1+\nu)\alpha\Delta T,$$
$$\sum_{n=0}^{\infty} h_n^J(q_L,\xi_i,\eta)A_n + \sum_{n=0}^{\infty} h_n^N(q_L,\xi_i,\eta)B_n + \sum_{n=1}^{\infty} l_n^J(q_T,\xi_i,\eta)C_n + \sum_{n=1}^{\infty} l_n^N(q_T,\xi_i,\eta)D_n = 0 \tag{32}$$

with

$$\begin{aligned}
f_n^J(q_L,\xi,\eta) = & -\frac{(1-\nu)}{h^3}\frac{\partial h}{\partial \xi} Je_n'(q_L,\xi)Se_n(q_L,\eta) + \frac{(1-\nu)}{h^3}\frac{\partial h}{\partial \eta} Je_n(q_L,\xi)Se_n'(q_L,\eta)\\
& + \frac{1}{h^2}\big((1-\nu)\alpha_{L_n} - 2q_L(\cosh 2\xi - \nu\cos 2\eta)\big)Je_n(q_L,\xi)Se_n(q_L,\eta), \quad n = 0,\infty\\
f_n^N(q_L,\xi,\eta) = & -\frac{(1-\nu)}{h^3}\frac{\partial h}{\partial \xi} Ne_n'(q_L,\xi)Se_n(q_L,\eta) + \frac{(1-\nu)}{h^3}\frac{\partial h}{\partial \eta} Ne_n(q_L,\xi)Se_n'(q_L,\eta)\\
& + \frac{1}{h^2}\big((1-\nu)\alpha_{L_n} - 2q_L(\cosh 2\xi - \nu\cos 2\eta)\big)Ne_n(q_L,\xi)Se_n(q_L,\eta), \quad n = 0,\infty\\
g_n^J(q_T,\xi,\eta) = & -\frac{(1-\nu)}{h^3}\frac{\partial h}{\partial \xi} Jo_n(q_T,\xi)So_n'(q_T,\eta) - \frac{(1-\nu)}{h^3}\frac{\partial h}{\partial \eta} Jo_n'(q_T,\xi)So_n(q_T,\eta)\\
& + \frac{(1-\nu)}{h^2} Jo_n'(q_T,\xi)So_n'(q_T,\eta), \quad n = 1,\infty\\
g_n^N(q_T,\xi,\eta) = & -\frac{(1-\nu)}{h^3}\frac{\partial h}{\partial \xi} No_n(q_T,\xi)So_n'(q_T,\eta) - \frac{(1-\nu)}{h^3}\frac{\partial h}{\partial \eta} No_n'(q_T,\xi)So_n(q_T,\eta)\\
& + \frac{(1-\nu)}{h^2} No_n'(q_T,\xi)So_n'(q_T,\eta), \quad n = 1,\infty\\
h_n^J(q_L,\xi,\eta) = & -\frac{1}{h^2}\frac{\partial h}{\partial \eta} Je_n'(q_L,\xi)Se_n(q_L,\eta) - \frac{1}{h^2}\frac{\partial h}{\partial \xi} Je_n(q_L,\xi)Se_n'(q_L,\eta)\\
& + \frac{1}{h} Je_n'(q_L,\xi)Se_n'(q_L,\eta), \quad n = 0,\infty\\
h_n^N(q_L,\xi,\eta) = & -\frac{1}{h^2}\frac{\partial h}{\partial \eta} Ne_n'(q_L,\xi)Se_n(q_L,\eta) - \frac{1}{h^2}\frac{\partial h}{\partial \xi} Ne_n(q_L,\xi)Se_n'(q_L,\eta)\\
& + \frac{1}{h} Ne_n'(q_L,\xi)Se_n'(q_L,\eta), \quad n = 0,\infty\\
l_n^J(q_T,\xi,\eta) = & -\frac{1}{h^2}\frac{\partial h}{\partial \eta} Jo_n(q_T,\xi)So_n'(q_T,\eta) + \frac{1}{h^2}\frac{\partial h}{\partial \xi} Jo_n'(q_T,\xi)So_n(q_T,\eta)\\
& - \frac{1}{h}\big(\beta_{T_n} - q_T(\cos 2\eta + \cosh 2\xi)\big)Jo_n(q_T,\xi)So_n(q_T,\eta), \quad n = 1,\infty\\
l_n^N(q_T,\xi,\eta) = & -\frac{1}{h^2}\frac{\partial h}{\partial \eta} No_n(q_T,\xi)So_n'(q_T,\eta) + \frac{1}{h^2}\frac{\partial h}{\partial \xi} No_n'(q_T,\xi)So_n(q_T,\eta)\\
& - \frac{1}{h}\big(\beta_{T_n} - q_T(\cos 2\eta + \cosh 2\xi)\big)No_n(q_T,\xi)So_n(q_T,\eta), \quad n = 1,\infty
\end{aligned}$$

The calculation of the displacement field, given in Eq. (28), needs the resolution of both systems of Eq. (32) (expressed on the boundaries ξ_1 and ξ_2) in order to determine the unknown coefficients A_n, B_n, C_n and D_n.

2.4. Resolution of the differential equations for a full elliptic plate

The vibration of a full elliptic plate is treated as a particular case of the hollowed plate vibration. Here, the interior boundary ξ_1 is zero and the exterior one becomes ξ_0. Considering the fact that the plate is full, the

displacement in its center is finite and continuous. Consequently, the solutions of the radial Mathieu equations can only be of the first kind [2,21].

Under the same previous hypothesis of excitation and displacement symmetry, the displacement field is simply deduced from the one corresponding to the hollowed plate case, given in Eq. (28), by setting to zero the coefficients B_n, and D_n:

$$U_\xi(\xi,\eta) = \frac{1}{h}\sum_{n=0}^{\infty} A_n Je'_n(q_L,\xi)Se_n(q_L,\eta) + \frac{1}{h}\sum_{n=1}^{\infty} C_n Jo_n(q_T,\xi)So'_n(q_T,\eta),$$
$$U_\eta(\xi,\eta) = \frac{1}{h}\sum_{n=0}^{\infty} A_n Je_n(q_L,\xi)Se'_n(q_L,\eta) - \frac{1}{h}\sum_{n=1}^{\infty} C_n Jo'_n(q_T,\xi)So_n(q_T,\eta), \tag{33}$$

where the coefficients A_n and C_n are determined by taking into account the boundary conditions expressed by the system of Eq. (32) and adapted to the case of a full plate,

$$\begin{aligned} &\sum_{n=0}^{\infty} f_n^J(q_L,\xi_0,\eta)A_n + \sum_{n=1}^{\infty} g_n^J(q_T,\xi_0,\eta)C_n = (1+\nu)\alpha\Delta T, \\ &\sum_{n=0}^{\infty} h_n^J(q_L,\xi_0,\eta)A_n + \sum_{n=1}^{\infty} l_n^J(q_T,\xi_0,\eta)C_n = 0, \end{aligned} \qquad \xi = \xi_0. \tag{34}$$

3. Numerical calculation of displacement fields

As mentioned before, the displacement field will be calculated only for a uniform microwave excitation. The angular dependence of the in-plane displacement of elliptic plates imposes the satisfaction of the zero stress conditions in the totality of the boundaries. In practice, the boundaries of a quarter of the plate will be discretized with respect to the angular variable η in order to satisfy the system of Eqs. (32) or (34) in each discretization point, depending on the geometry of the plate (see Fig. 2). In the following development, the calculation of the displacement field in hollowed plates is presented in details. In the case of full plates, the number of boundaries, and consequently the size of vectors and matrix, changes while the resolution method remains unchanged.

As represented in Fig. 2(b), the boundary of the hollowed elliptic plate is discretized into $2N$ points (N point for each border), where the system of Eq. (32) is verified. The total number of equations equals $4N$ and, in order to obtain a square system of equations, the infinite series are truncated until the Nth unknown. The discretized system will consequently take the following:

$$\mathbf{M}(\xi_1,\xi_2,\eta_i,\omega)\cdot\mathbf{A} = \mathbf{b}, \tag{35}$$

where i is the calculation point index which varies from 1 to N, $\mathbf{M}(\xi_1,\xi_2,\eta_i,\omega)$ is a square matrix ($4N\times 4N$) composed of the functions f_n, g_n, h_n and l_n given in Eq. (32) and evaluated at each point of both boundaries,

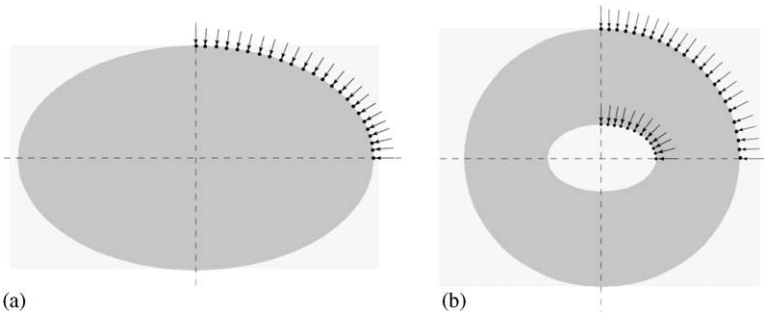

Fig. 2. Discretization of elliptic plate boundaries of: (a) a full elliptic plate and (b) a hollowed elliptic plate, submitted to a uniform temperature elevation.

A is a $4N$ vector containing the unknown coefficients A_n, B_n, C_n and D_n, and **b** is a second member vector, of dimension $4N$, that contains the terms of the uniform thermal excitation.

The resolution of the algebraic system of Eq. (35) furnishes the researched set of coefficients and allows calculating the displacement field given by Eq. (28).

4. Experimental setup

The experimental setup, schematized in Fig. 3, allows exciting structures by pulsed microwave irradiations. A magnetron, working at the frequency of 9.41 GHz with a peak power of 5.5 kW, produces a 1 μs electromagnetic pulse or bursts made of n pulses. The number n and the repetition frequency f_{rep} of the pulses are chosen with a function generator (Agilent 33120A). The quasi-impulsional responses of the tested structures can be obtained with a single pulse since its frequency range is much larger than the frequency spectrum of the studied samples. By using a burst, the resonances of the samples can be excited by adjusting the pulses repetition frequency f_{rep} in the burst to particular resonance frequencies.

The generated microwaves propagate into a rectangular waveguide, of interior dimensions $23 \times 10\,mm^2$, where the fundamental electromagnetic mode is TE_{10}.

In order to obtain a maximum power in the sample, an impedance adaptor is adjusted to get the minimum reflected power, which is measured, with a wattmeter. A circulator permits to direct the microwaves reflected by the sample to the detector and finally to the wattmeter.

The particular velocity on the surface of the sample is measured with a Laser velocimeter (Polytec OFV 353) related to a modular controller (Polytec OFV 3001) with a sensitivity of 5 mm/s/V in a frequency bandwidth limited to 250 kHz. The signal is acquired and averaged, through a filtering amplifier (Electronic Instrument 3627), by a numerical oscilloscope (LeCroy 9450A) and sent to a computer to be treated. Finally, the measured temporal velocity is Fourier transformed to obtain the sample spectral response.

Four elliptic plates have been designed using epoxy-based resins charged with graphite. Indeed, graphite enhances the microwaves absorption and the temperature rise in order to maximize the vibration amplitude of the tested samples. The names, the interior and exterior semi-axes and the exterior boundary eccentricities of the full and the hollowed plates are given in Table 1.

The epoxy resin is viscoelastic. In order to take into account the dissipative aspect of the wave propagation, a complex Young's modulus, for which the imaginary part represents the damping of the material, is used. The Young's modulus E and the Poisson's ratio ν have been evaluated using an evaluation method based on the eigenfrequencies of a disk made of the same epoxy resin [19]. The imaginary part of the Young's modulus has been estimated by tests performed on a road made of the same material [17]. The obtained material properties

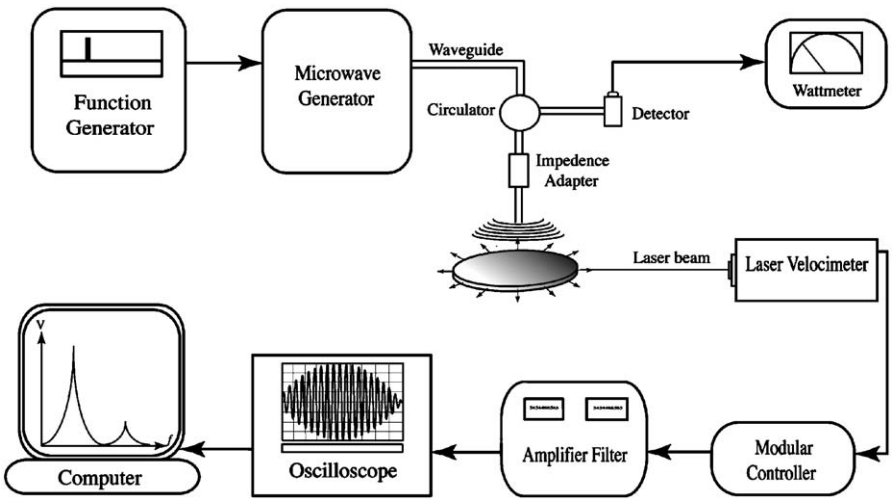

Fig. 3. Experimental setup for exciting and measuring the vibrations of samples submitted to microwaves irradiations.

Table 1
Geometrical properties of the designed full and hallowed elliptic plates

	Name	a_{ext} (mm)	b_{ext}(mm)	a_{int} (mm)	b_{int} (mm)	$e_{ext} = f/a_{ext}$ (%)
Full ellipses	FE_1	31.5	20.0	—	—	77.3
	FE_2	38.0	30.0	—	—	61.4
Hollowed ellipses	HE_1	31.5	30.0	14.0	10.3	30.5
	HE_2	38.0	36.0	20.0	15.9	32.0

of the four samples are $E(3.65+0.10\mathrm{i})$ Gpa and $v = 0.39$ with accuracies, respectively, equal to 2.0% and 2.5%. The measured density of the plate-based material is 1140 kg/m^3. Finally, since the thicknesses of the tested plates are equal to 3 mm, the temperature variation in their depth is estimated to be less then 0.5% [11].

5. Experimental results and model validation

The earlier developed models will be compared to the experimental results in order to be validated. Since, the experimental excitation durations are very small comparing to the vibration periods of the studied plates, the corresponding responses are considered as impulsional ones. Remembering that the experimental setup permits the measurement of velocity, one can choose to compare the experimental and the theoretical velocity spectra corresponding to a sudden microwave excitation. The analytical velocity is obtained by derivation, in the frequency domain, of the displacement given by Eqs. (33) and (28):

$$\dot{\mathbf{U}}(\xi,\eta) = \mathrm{i}\omega\mathbf{U}(\xi,\eta). \tag{36}$$

Fig. 4 shows the superposition of the experimental and the theoretical velocity spectra at the boundary of the plate FE_1 at positions $\eta = 0^\circ$ and 90°. Similarly, in Fig. 5 are represented the experimental and the theoretical velocity spectra at positions $\eta = 0^\circ$ and 90° of the boundary of the plate FE_2.

The superposition of the theoretical and the experimental spectra shows a good correlation between the responses predicted by the model and the experimental ones. The relative amplitudes of particular velocities obtained analytically and experimentally do not perfectly coincide because of the indetermination in the exact distribution of the microwave field which is, experimentally, axisymmetric rather than uniform. This causes the generation of certain modes that appear in the experimental spectra but that are not taken into account by the theoretical model. Furthermore, the residual noise contained in the experimental signals introduces an inaccuracy on the measured amplitudes.

The differences between the theoretical and the experimental eigenfrequencies, observable in Figs. 4 and 5, could be due to the truncate error of the infinite Mathieu series in the model. This truncate error also causes the apparition of some fictitious eigenfrequencies. Moreover, the experimental eigenfrequencies are sensitive to the support conditions when the wavelengths decrease because of the apparition of friction between the sample and the support. This phenomenon also explains the differences between theoretical and experimental results at high frequencies since the model does not take into account the friction behavior.

However, Figs. 4 and 5 show that the vibration of the full elliptic plates FE_1 and FE_2 is well predicted by the above developed model in spite of the ellipse strong eccentricities which are, respectively, equal to 77.3% and 61.4%. Finally, the model has served to calculate the deformed shape of the plate FE_1 corresponding to its first seven eigenfrequencies obtained by a uniform thermal excitation. The superposition of these deformed shapes with the original elliptic shape of the plate FE_1 is given in Fig. 6. In addition to the symmetry of the displacement, one can observe that the number of curvatures in the plate boundary increases with respect to the eigenfrequency value.

Figs. 7 and 8 show the comparison between the theoretical and the experimental velocity spectra of the plates HE_1 and HE_2 at the two angular positions $\eta = 0^\circ$ and 90° of the external boundaries. One can observe that the coincidence between the model and the experimental results in this case is globally good but not as accurate as in the full plate case. This is due to experimental and modeling reasons.

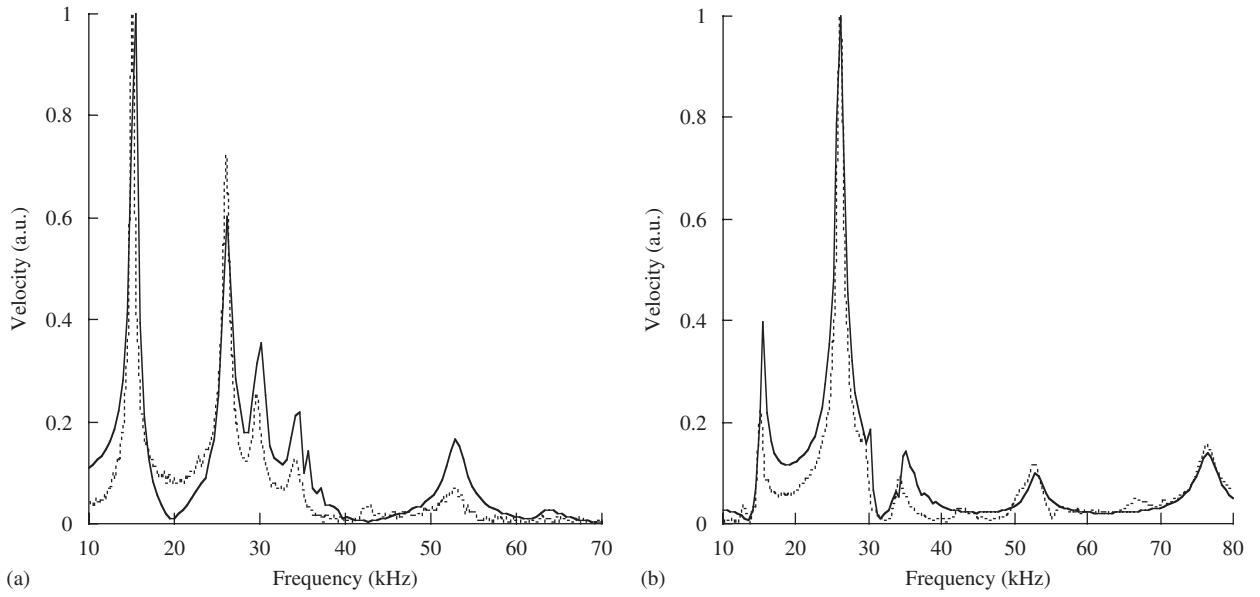

Fig. 4. Comparison of experimental and theoretical velocity spectra of the plate FE_1 at the angular positions (a) $\eta = 0^\circ$ and (b) $\eta = 90^\circ$ of the boundary. · · · · · · · · · · · · · · Experimental, ——— theoretical.

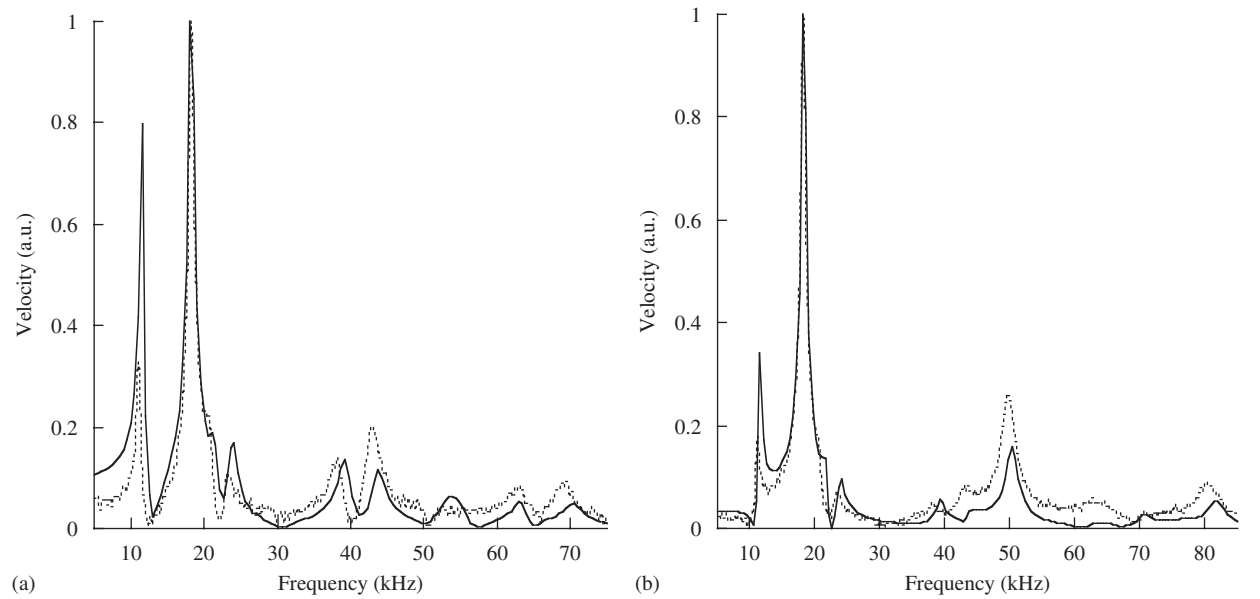

Fig. 5. Comparison of experimental and theoretical velocity spectra of the plate FE_2 at the angular positions (a) $\eta = 0^\circ$ and (b) $\eta = 90^\circ$ of the boundary. · · · · · · · · · · · · · · Experimental, ——— theoretical.

On the one hand, the rectangular waveguide used to excite the hollowed plates is not geometrically adapted to uniformly excite the hollowed plates. Indeed, the dimensions of the rectangular waveguide are smaller than the dimensions of the holes, particularly in the case of the plate HE_2 (see Table 1). Consequently, the irradiation is not sufficient to excite a large volume in the plate and to obtain a satisfactory mechanical response with a good signal-to-noise ratio (see Figs. 7(a) and 8(b)). One possible solution is to adapt the geometry of the waveguide by increasing its dimensions with respect to the dimensions of the studied plates.

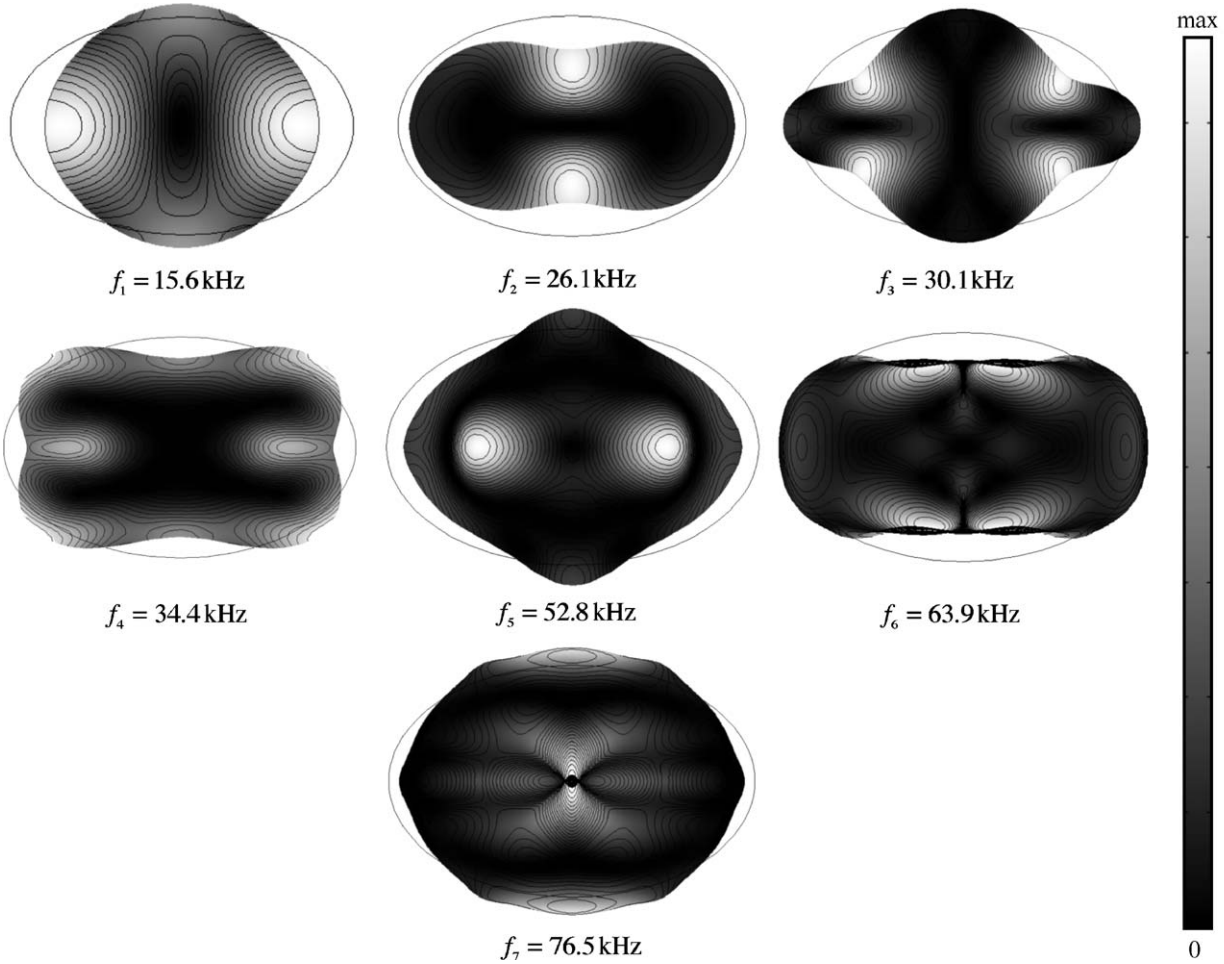

Fig. 6. Representation of the deformed shapes, in term of displacement, of the first seven eigenmodes of the plate FE_1 obtained theoretically by a uniform thermal excitation. The maximum displacements are represented in white color and the displacement isolines are given by the plain lines.

On the other hand, the discretization of two boundaries strongly increases the size of the matrix to be inversed in Eq. (35). Since the inversion of large and full matrices is numerically difficult, the theoretical velocity field in an elliptic hollowed plate is less accurate than in a full one. The use of a pseudo-inverse algorithm (Moore–Penrose least-squares method [26]) has increased the accuracy in the case of the full elliptic plates (Figs. 4 and 5) but has not provided better results in the case of the hollowed plates (Figs. 7 and 8). In addition, one can observe that the theoretical and the experimental spectra of the plate HE_1 are well correlated comparing to those of the plate HE_2. This is due to the strong sensitivity of the numerical resolution algorithm to the eccentricities of the exterior elliptic boundaries (e_{ext}) of the hollowed plates HE_1 and HE_2 (respectively, equal to 30.5% and 32.0%). Indeed, the more the eccentricity is high (the more the ellipse curve is high), the more the displacement fields need calculation accuracy, otherwise numerical noise appears.

Nevertheless, Figs. 7 and 8 permit to conclude that the model of hollowed plate vibrations is valid under the above experimental and numerical conditions.

6. Conclusions

The in-plane free vibration of elliptic plates using microwave acoustic generation technique has been successfully studied. A two-dimensional semi-analytical model that predicts the in-plane vibration of such

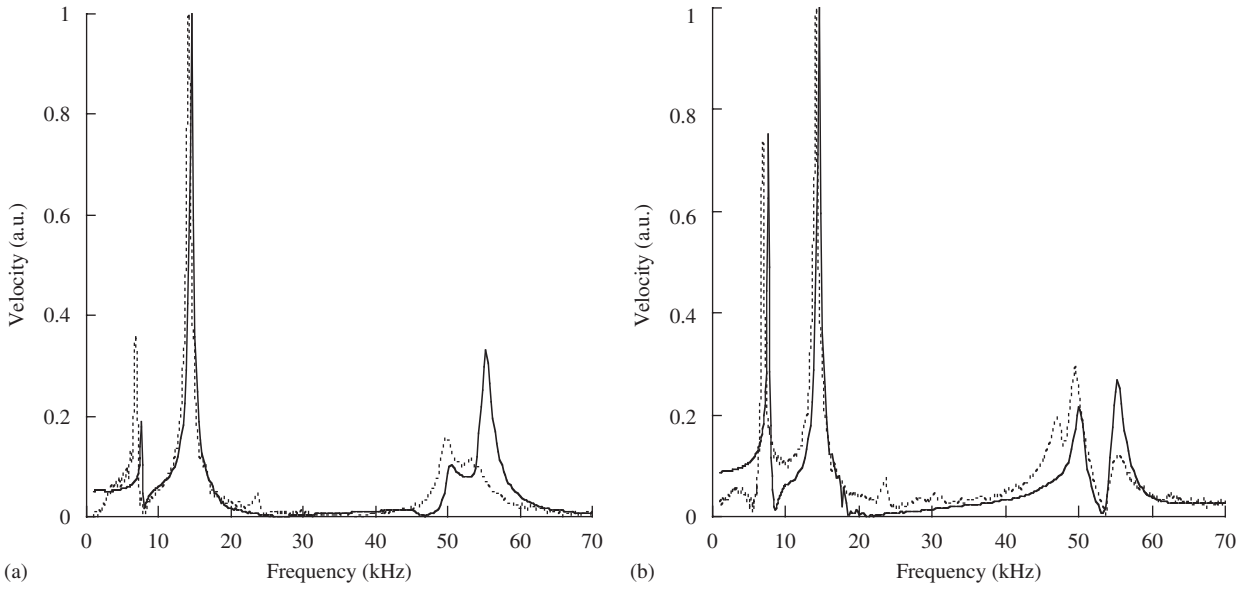

Fig. 7. Comparison of experimental and theoretical velocity spectra of the plate HE_1 at the angular positions (a) $\eta = 0^\circ$ and (b) $\eta = 90^\circ$ of the external boundary. · · · · · · · · · · · · · · Experimental, ——— theoretical.

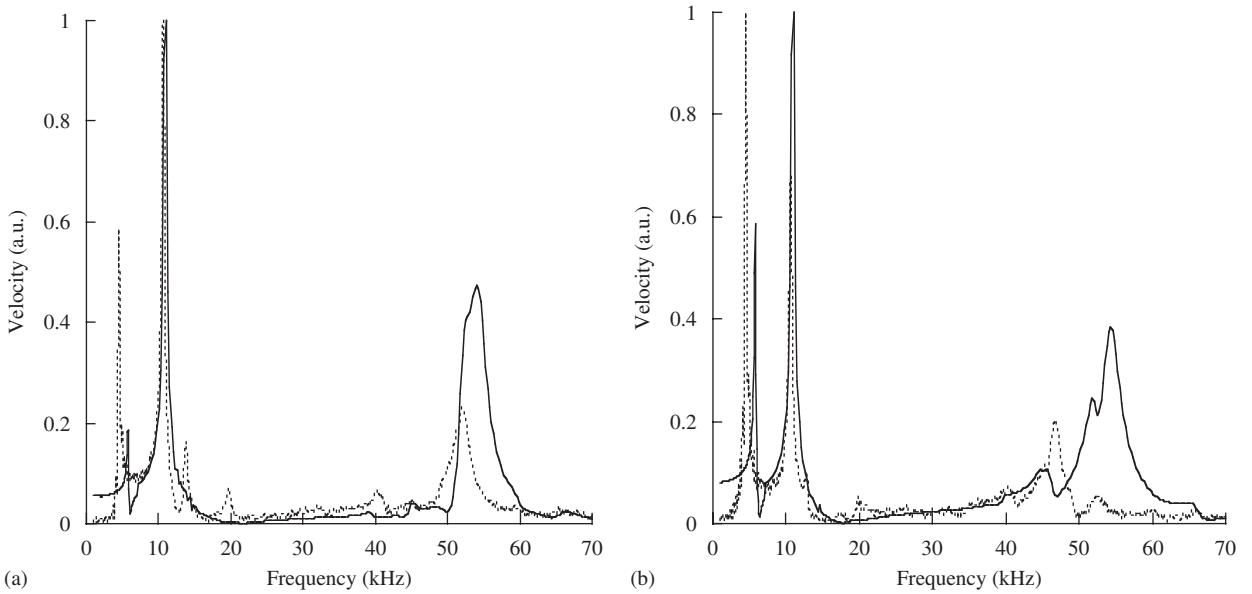

Fig. 8. Comparison of experimental and theoretical velocity spectra of the plate HE_2 at the angular positions (a) $\eta = 0^\circ$ and (b) $\eta = 90^\circ$ of the external boundary. · · · · · · · · · · · · · · Experimental, ——— theoretical.

structures has been developed by solving Helmholtz equations in elliptic cylindrical coordinates using Mathieu function series.

The satisfactory comparison between theoretical and experimental responses has validated the modeling of full and hollowed elliptic plates vibration. In addition, this comparison has permitted to highlight some numerical inaccuracies related to the curve of the elliptic plates. A possible perspective is to investigate numerical methods, as inversion algorithms and linear optimization, to get round these difficulties.

Contrary to other analytical studies of the in-plane vibration of elliptic plates, the model applied to microwave generation allows predicting not only the eigenfrequencies but also the spectrum amplitude with a quite good accuracy. The microwave generation technique permits the experimental generation of the in-plane vibration of thin plates with a very good reproducibility, and allows to carry out the experimental validation of modeling. It has been shown that the experimental setup has to be adapted to the dimensions of the studied samples in order to increase the signal-to-noise ratio of the mechanical response.

As an application of the present work, one can imagine to use the model developed here and the microwave generation method to characterize the geometry of elliptic plates by solving the related inverse problem. This is made possible since the semi-analytical resolution method presented in this paper is faster than a purely numerical method like FEM. In this sense, the technique of microwave acoustic generation coupled with the present model can serve to perform the non-destructive characterization of elliptic plates in general and of circular ones in particular (since the circular structures are particular cases of the elliptic ones). Moreover, the effect of a small ellipticity on the accuracy of the characterization method described in Ref. [19] (which is based on the eigenfrequencies of a perfectly circular thin plate) could be studied using this new model. A possible perspective to the present work is to study the acoustic generation of an elliptic hole in an infinite plate by means of an asymptotic analysis. This could be interesting in the non-destructive investigation of plate defects that can be geometrically approached by ellipses. Finally, as mentioned in the paper, this study can be easily extended to the case of infinite elliptic cylinders by replacing the plane stress hypothesis by a plane strain assumption. In bioacoustics, for example, this extension could be used to model the acoustical response of a human bone (which can be approached by a hollowed elliptic tube) submitted to uniform and longitudinal microwave irradiations.

Acknowledgments

The authors are very grateful to Dr. M. Deschamps for his helpful advices in achieving the present study.

References

[1] E. Mathieu, Mémoire sur le mouvement vibratoire d'une membrane de forme elliptique, *Journal de Mathématiques Pures et Appliquées* 13 (1868) 137–203.
[2] J.C. Gutiérrez-Vega, S. Chávez-Cerda, R.M. Rodríguez-Dagnino, Free oscillations in an elliptic membrane, *Revista Mexicana de Fisica* 45 (6) (1999) 613–622.
[3] K. Hong, J. Kim, Natural mode analysis of hollow and annular elliptical cylindrical cavities, *Journal of Sound and Vibration* 183 (2) (1995) 327–351.
[4] W.R. Callahan, Flexural vibrations of elliptical plates when transverse shear and rotary inertia are considered, *Journal of Acoustical Society of America* 36 (5) (1964) 823–829.
[5] W.R. Callahan, Frequency equations for the normal modes of vibration for an elliptical ring, including transverse shear and rotary inertia, *Journal of Acoustical Society of America* 37 (3) (1965) 480–485.
[6] K. Sato, Free flexural vibrations of an elliptical plate with simply supported edge, *Journal of Acoustical Society of America* 52 (3B) (1972) 919–922.
[7] A.W. Leissa, Vibration of a simply-supported elliptical plate, *Journal of Sound and Vibration* 6 (1) (1967) 145–148.
[8] R. Barakat, Diffraction of plane waves by an elliptic cylinder, *Journal of Sound and Vibration* 35 (12) (1963) 1990–1996.
[9] P.K. Wong, J. Miklowitz, R.A. Scott, Propagation of harmonic flexural waves in an infinite elastic rod of elliptical cross-section, *Journal of Acoustical Society of America* 40 (2) (1966) 393–398.
[10] B. Hosten, P. Alain Bernard, Ultrasonic wave generation by time gated microwaves, *Journal of Acoustical Society of America* 70 (1998) 1577–1585.
[11] C. Bacon, B. Hosten, P.A. Bernard, Acoustic wave generation in viscoelastic rods by time-gated microwaves, *Journal of Acoustical Society of America* 106 (1999) 195–201.
[12] C. Bacon, B. Hosten, E. Guilliorit, One dimensional prediction of the acoustic waves generated in a multilayer viscoelastic body by microwave irradiation, *Journal of Sound and Vibration* 238 (5) (2000) 853–867.
[13] C. Bacon, E. Guilliorit, B. Hosten, D. Chimenti, Acoustic waves generated by pulsed microwaves in viscoelastic rods: modeling and experimental verification, *Journal of Acoustical Society of America* 110 (3) (2001) 1398–1407.
[14] B. Hosten, C. Bacon, Measurement of complex Young moduli of composite materials by time gated microwaves, *Review of Progress in Quantitative Nondestructive Evaluation*, vol. 19(1), Plenum Press, New York, 2000, pp. 1113–1120.
[15] E. Guilliorit, C. Bacon, B. Hosten, Prediction of the Generation of Acoustic Waves due to the Penetration of Pulsed Microwaves in Multilayer Media, *Journal of Acoustical Society of America* 112 (1) (2002) 65–74.

[16] E. Guilliorit, B. Hosten, C. Bacon, D.E. Chimenti, Microwave excitation of ultrasound in graphite-fiber reinforced composite plates, *Ultrasonics* 41 (2003) 97–103.
[17] C. Bacon, E. Guilliorit, B. Hosten, An acoustic-microwave method for the study of the mechanical influence of moisture content in materials, *Journal of Applied Mechanics* 70 (2003) 268–274.
[18] A.R. Hadj Henni, C. Bacon, B. Hosten, Acoustic generation in piezoelectric materials by microwave excitation, *Journal of Acoustical Society of America* 118 (4) (2005) 2281–2288.
[19] A.R. Hadj Henni, C. Bacon, B. Hosten, In-plane vibration of thin circular structures submitted to pulsed microwave irradiations, *Journal of Acoustical Society of America* 119 (6) (2006) 3782–3792.
[20] M.R. Spiegel, *Mathematical Handbook of Formulas and Tables*, McGraw-Hill, New York, 1974.
[21] P.M. Morse, H. Feshbach, *Methods of Theoretical Physics*, vols. 1, 2, McGraw-Hill, New York, 1953.
[22] J.D. Achenbach, *Wave Propagation in Elastic Solids*, North-Holland, Amsterdam, 1973.
[23] M. Abramowitz, I.A. Stegun, *Handbook of Mathematical Functions—With Formulas, Graphs and Mathematical Tables*, Dover Publications, Inc., New York, 1965.
[24] Julio.C. Gutiérrez-Vega, R.M. Rodríguez-Dagnino, M.A. Meneses-Nava, S. Chávez-Cerda, Mathieu functions a visual approach, *American Journal of Physics* 71 (2003) 233–242.
[25] S. Zhang, J.M. Jin, *Computation of Special Functions*, Wiley, New York, 1996.
[26] *Matlab® User's Guide*, Mathworks, Inc., Natick, MA 〈http://www.mathworks.com〉.